Clinical Cancer Research

Activity of MM-398, Nanoliposomal Irinotecan (nal-IRI), in Ewing's Family Tumor Xenografts Is Associated with High Exposure of Tumor to Drug and High *SLFN11* Expression

Min H. Kang[1,2], Jing Wang[1,2], Monish R. Makena[1,2], Joo-Sang Lee[1,2], Nancy Paz[3], Connor P. Hall[1,2], Michael M. Song[1,2], Ruben I. Calderon[1,2], Riza E. Cruz[1,2], Ashly Hindle[1,2], Winford Ko[1,2], Jonathan B. Fitzgerald[3], Daryl C. Drummond[3], Timothy J. Triche[4], and C. Patrick Reynolds[1,2]

Abstract

Purpose: To determine the pharmacokinetics and the antitumor activity in pediatric cancer models of MM-398, a nanoliposomal irinotecan (nal-IRI).

Experimental Design: Mouse plasma and tissue pharmacokinetics of nal-IRI and the current clinical formulation of irinotecan were characterized. *In vivo* activity of irinotecan and nal-IRI was compared in xenograft models (3 each in nu/nu mice) of Ewing's sarcoma family of tumors (EFT), neuroblastoma (NB), and rhabdomyosarcoma (RMS). *SLFN11* expression was assessed by Affymetrix HuEx arrays, Taqman RT-PCR, and immunoblotting.

Results: Plasma and tumor concentrations of irinotecan and SN-38 (active metabolite) were approximately 10-fold higher for nal-IRI than for irinotecan. Two doses of NAL-IRI (10 mg/kg/dose) achieved complete responses maintained for >100 days in 24 of 27 EFT-xenografted mice. Event-free survival for mice with RMS and NB was significantly shorter than for EFT. High *SLFN11* expression has been reported to correlate with sensitivity to DNA damaging agents; median *SLFN11* mRNA expression was >100-fold greater in both EFT cell lines and primary tumors compared with NB or RMS cell lines or primary tumors. Cytotoxicity of SN-38 inversely correlated with *SLFN11* mRNA expression in 20 EFT cell lines.

Conclusions: In pediatric solid tumor xenografts, nal-IRI demonstrated higher systemic and tumor exposures to SN-38 and improved antitumor activity compared with the current clinical formulation of irinotecan. Clinical studies of nal-IRI in pediatric solid tumors (especially EFT) and correlative studies to determine if *SLFN11* expression can serve as a biomarker to predict nal-IRI clinical activity are warranted. *Clin Cancer Res; 21(5); 1139–50. ©2015 AACR.*

Introduction

Irinotecan hydrochloride, a water-soluble analogue of the natural alkaloid camptothecin (CPT; ref. 1), is first-line therapy in combination with 5-fluorouracil (5-FU) and leucovorin for metastatic colorectal cancer (2, 3). Carboxylesterase catalyzes irinotecan into SN-38, which is >100-fold more cytotoxic than irinotecan against tumor cells *in vitro* (4, 5). However, the complicated pharmacology of irinotecan has likely limited its clinical activity. An active lactone form spontaneously hydrolyzes into the inactive carboxylate form in normal physiologic pH until the carboxylate form reaches equilibrium (~30% of total irinotecan; refs. 6, 7). Other pharmacologic disadvantages of irinotecan include fast elimination of the drug (8, 9), and diarrhea, due to β-glucuronidases produced by intestinal microflora that mediate hydrolysis of SN-38 glucuronide (inactive phase II metabolite of SN-38) to form the active metabolite SN-38 (10).

Liposomal formulations of irinotecan have been introduced (11, 12), which slow elimination and minimize exposure of the drug to serum (which at neutral to basic pH promotes hydrolysis of irinotecan), and thus stabilize the active lactone form versus the inactive carboxylate form (13). A nanoliposomal formulation of irinotecan, nal-IRI (also known as MM-398 or PEP02), employs a modified gradient loading method with sucrose octasulfate (13). Macrophage-mediated disruption of the nal-IRI, drug release, and conversion to SN-38 for *in vivo* require >24 hours, and preclinical studies demonstrated activity against colorectal and breast cancer subcutaneous xenografts (13), as well as intracranial glioblastoma tumor xenografts (14–16). A three-arm phase II study of nal-IRI versus irinotecan or docetaxel as a second-line therapy in patients with locally advanced or metastatic gastric or gastro-esophageal junction adenocarcinoma demonstrated an objective response rate comparable with docetaxel (17). A nal-IRI phase II study in

[1]Cancer Center, School of Medicine, Texas Tech University Health Sciences Center, Lubbock, Texas. [2]Departments of Cell Biology and Biochemistry, School of Medicine, Texas Tech University Health Sciences Center, Lubbock, Texas. [3]Merrimack Pharmaceuticals, Cambridge, Massachusetts. [4]Department of Pathology Keck School of Medicine, University of Southern California, Los Angeles, California.

Note: Supplementary data for this article are available at Clinical Cancer Research Online (http://clincancerres.aacrjournals.org/).

Corresponding Author: C. Patrick Reynolds, School of Medicine, Texas Tech University Health Sciences Center, 3601 4th Street STOP 9445 Lubbock, TX 79430. Phone: 806-743-1558; Fax: 806-743-2691; E-mail: Patrick.reynolds@ttuhsc.edu

doi: 10.1158/1078-0432.CCR-14-1882

Translational Relevance

Despite high *in vitro* activity of the irinotecan active metabolite (SN-38), chemical and pharmacokinetic properties of irinotecan have potentially limited clinical activity. A nanoliposomal formulation of irinotecan (nal-IRI) with improved pharmacokinetic properties relative to irinotecan was developed, and is being tested in clinical trials. We demonstrated for nal-IRI compared with irinotecan advantageous pharmacokinetic properties and significantly greater antitumor activity in mouse xenograft models of pediatric solid tumors, especially in Ewing's sarcoma family of tumors (EFT). Expression of *SLFN11*, a putative DNA/RNA helicase, correlated with the *in vitro* activity of SN-38. In a panel of cell lines and in primary tumors, *SLFN11* mRNA expression was significantly higher for EFT relative to neuroblastoma or rhabdomyosarcomas. Our data confirm that nal-IRI improves systemic and tumor exposure to irinotecan and its active metabolite in murine xenograft models of childhood solid tumors, leading to enhanced antitumor activity. The high expression of *SLFN11* in EFT suggests a molecular mechanism for the striking activity of nal-IRI in EFT xenografts and provides a potential marker for drug sensitivity in clinical trials including an on-going phase I clinical trial of nal-IRI (SPOC-2012-001;NCT 02013336).

patients with metastatic, gemcitabine-refractory pancreatic cancer achieved a one-year survival rate of 25% (18). Nal-IRI combined with 5-FU and leucovorin demonstrated significantly improved overall survival for gemcitabine-refractory pancreatic cancer patients compared with 5-FU/leucovorin alone in a recently completed phase III pivotal trial (NAPOLI-1; ref. 19).

Here, we report the comparative pharmacokinetic profiles and antitumor activity in mouse xenograft models of pediatric solid tumors of nal-IRI and irinotecan (Camptosar). High expression of *SLFN11* has been reported for Ewing's family of tumors (20), and *SLFN11* expression has been associated with sensitivity to cytotoxic agents (21). Therefore, we also examined the correlation between *in vitro* activity of SN-38 and *SLFN11* expression in panels of pediatric cancer cell lines, the relative expression of *SLFN11* in pediatric primary tumors, and the correlation of *SLFN11* expression with the Ewing's-specific aberrant transcription factor EWS/FLI (22).

Materials and Methods

Drugs and chemicals

Merrimack Pharmaceuticals provided nal-IRI (nanoliposomal irinotecan·HCl, 5.0 mg/mL). Irinotecan (Camptosar, 20 mg/mL, free drug formulation) was from Baxter Healthcare Corporation. 4-HC was purchased from Niomech (Germany), and cyclophosphamide for *in vivo* studies was from Baxter. Topotecan, pure irinotecan·HCl, SN-38 (active metabolite of irinotecan), camptothecin (internal standard: IS), and all other chemicals were LC-MS grade and were purchased from Sigma-Aldrich Chemical Company. Methanol and acetonitrile were from Fisher Scientific. Normal mouse plasma was from Lampire Biological Laboratories and filtered by 6 mL charcoal packing Resprep SPE cartridges (Restek). Drug-free human plasma was obtained from the TTUHSC Blood Bank.

Cell lines

For these studies, we employed 20 Ewing's sarcoma (EFT), 20 neuroblastoma (NB), and 12 rhabdomyosarcoma (RMS) cell lines that were established in our laboratory or obtained from the originator of the line (Supplementary Table S1). All cell lines were grown in antibiotic-free RPMI-1640 supplemented with 10% heat-inactivated FBS or Iscoves Modified Dulbeccos Medium (IMDM) supplemented with 3 mmol/L $_L$-glutamine, 5 μg/mL insulin, and 20% heat-inactivated FBS, were mycoplasma free, and were cultured and treated with drugs in a 37°C incubator with 5% CO_2. Cell line identity was confirmed at the time of experimentation by short tandem repeat (STR) genotyping (23) and compared with the Children's Oncology Group STR database (www.COGcell.org).

Plasma, tissue, and tumor pharmacokinetics

All animal studies were approved by the Animal Care and Use Committee at TTUHSC. Female BALB/c mice (6–8 weeks, 16–18 g) and nu/nu mice (6–8 weeks, 24–28 g) were from Charles River Laboratories. Irinotecan or nal-IRI was injected intravenously at 5, 10, or 20 mg/kg into the lateral tail vein of BALB/c mice once. Blood was collected by cardiac puncture at various time points under isoflurane anesthesia and centrifuged immediately at 15,700 × *g* for 5 minutes at 4°C to isolate the plasma. Organs were harvested, minced, mixed with 3 volumes of PBS, and homogenized on ice using a Tissue Tearor (BioSpec Products). Protein content in tissues was determined as previously described (24). Plasma and tissue homogenates were stored at −80°C until analyses.

For tumor pharmacokinetics, the human CHLA-136 neuroblastoma cell line (15×10^6 cells/100 μL) was injected subcutaneously into nu/nu mice and after 42 days irinotecan or nal-IRI was injected intravenously (20 mg/kg). Blood, organs, and tumors were collected and processed as described above 4, 24, and 48 hours after injection.

Pharmacokinetic analyses

The concentrations of irinotecan and SN-38 in mouse plasma and tissues were determined by an Agilent 1200 HPLC system (Agilent Technologies) and a Applied Biosystems 4000QTRAP LC-MS/MS system (Applied Biosystems) with data analysis software Analyst 1.42 (Applied Biosystems). Isocratic separation was achieved using 50% of methanol (0.1% formic acid) and 50% of 2 mmol/L ammonium formate in water (0.1% formic acid) on a 2.1 × 50 mm Waters XBridge C18 Column (3.5 μm; Waters) with a 2.0 × 4 mm Phenomenex Security Guard C18 cartridge (Phenomenex) at a flow rate of 0.3 mL/min. The retention times for irinotecan, SN-38, and internal standard (I.S.) were 1.20, 2.02, and 2.55 minutes, and the total run time was 6 minutes.

The column effluent was connected to an electrospray ionization interface operated in the positive mode (600°C and 3,000 V ionization voltage); nebulizer gas = 40 psi and turbo gas = 50 psi; collision-activated dissociation gas was set at medium and the curtain gas at 15 psi. The collision energies for irinotecan, SN-38, and camptothecin were 59, 37, and 33 EV, and the collision exit potential for the analytes were 12, 20, and 16 EV, respectively. The detection of the analytes was performed using multiple reaction monitoring. The transitions were m/z 588.4 → m/z 167.2 for irinotecan, m/z 393.2 → m/z 349.1 for SN-38, and m/z 348.8 → m/z 305.0 for camptothecin.

Plasma calibration standards of irinotecan were prepared at 1.0 to 500 ng/mL, and for SN-38 at 0.5 to 250 ng/mL in purified mouse plasma. Tissue calibrations of irinotecan and SN-38 were performed in blank mouse liver homogenate (1:3 dilution with PBS). Method validation was per FDA guidelines (http://www.fda.gov/CDER/Guidance/4252fnl.html). The regression parameters of slope, intercept, and correlation coefficient were calculated by least-squares linear-regression analysis using a weight factor of $1/x^2$. For noncompartmental analysis, the area under the concentration *versus* time curve ($AUC_{0\text{-inf}}$) was calculated by using the trapezoidal rule extrapolated to infinity. Calculations were as follows: elimination half-life: $T_{1/2} = 0.693/ke$; systemic clearance: CL_{tot} = dose/AUC); and apparent volume of distribution: Vd = Dose/($AUC_{0\text{-inf}} \times ke$).

Conversion of irinotecan to SN-38 in mouse and human plasma

Irinotecan was spiked into blank human and mouse plasma to achieve final concentrations of 0, 10, 20, 50, 100, 250, 500, 750, and 1,000 ng/mL, incubated at 37°C for 24 hours, and reaction terminated by adding 600 μL of ice-cold acetonitrile–methanol (1:1, 0.1% formic acid) and 2 μL of internal standard solution (camptothecin 5 μg/mL). The concentrations of SN-38 in plasma were determined by LC-MS/MS. V_{max} and K_m values were calculated using GraphPad Prism software.

Antitumor activity of nal-IRI in murine xenografts

Subcutaneous xenografts with human cell lines from EFT (CHLA-258, COG-E-352,CHLA-32, SK-N-MC, and CHLA-25; refs. 25), RMS [CB-NJR (26), SMS-CTR (27), and Rh30 (direct xenografts; ref. 28)], and neuroblastoma (CHLA-136, CHLA-79, and CHLA-119; ref. 29) were established in nu/nu mice. All cell lines were grown before xenograft implantation in antibiotic-free medium and verified to be free of mycoplasma (MycoAlert kit; Lonza) and cell line identity confirmed by STR at the time of experimentation (23). For each 6- to 8-week-old female athymic nu/nu mouse, 2.5 to 10 million tumor cells were mixed with RPMI-1640:Matrigel (1:1) and injected subcutaneously between the shoulder blades. Tumor volume was measured twice weekly (28, 30). Drug treatment (irinotecan or nal-IRI, 10 mg/kg/d, Monday and Thursday, a total of 2 doses were given) began when progressively growing tumors reached a mean of 150 mm^3. Mice were sacrificed when the tumor volume exceeded 1,500 mm^3 or serious morbidity was observed. To assess combination activity of nal-IRI + cyclophosphamide given in multiple doses, mice were treated for 4 weeks with intravenous nal-IRI 10 mg/kg/d, each Monday and Thursday, and intraperitoneal cyclophosphamide 25 mg/kg (every Monday).

Quantifying macrophage content in tumors

Chromogenic immunohistochemistry was conducted on 5-μm-thick tumor frozen sections on fresh cut slides. Slides were baked for 30 minutes at 65°C, soaked in xylene, rehydrated through 100% and 80% graded alcohols, and pretreated with proteinase K (Invitrogen) for 15 minutes at room temperature. All further steps were done at room temperature in a hydrated chamber. Slides were blocked using Peroxidazed1 (Biocare) and serum-free protein block (Dako) to quench endogenous peroxidase activity, and nonspecific binding, respectively, stained overnight with the F4/80 antibody (Serotec, MCA497G, 1.0 mg/mL) incubated at a 1:1,000 dilution, and was developed using the rat on mouse HRP polymer kit (Biocare) as per the manufacturer and counterstained with hematoxylin. Slides were imaged on an Aperio Brightfield microscope at a 20× magnification. The percentage of macrophage-positive area was quantified as a ratio of total viable tumor tissue area was carried out using Definiens Tissue Studio XD (Definiens).

SLFN11 expression in association with sensitivity to SN-38

We assessed cytotoxicity of SN-38 using the DIMSCAN cytotoxicity assay as previously described (31, 32) and *SLFN11* expression by Taqman real-time reverse transcription-PCR (RT-PCR) as previously described (33) using primers and a probe from Applied Biosystems in 20 EFT, 20 NB, and 12 RMS cell lines (Supplementary Table S1). Relative IC_{50} (rIC_{50}) was calculated based on NCI Pediatric Preclinical Testing Program (PPTP) guidelines (32). *SLFN11* expression was also measured by Human Exon (HuEx) 1.0 ST Array (Affymetrix) in 17 EFT cell lines and expression measured by HuEx arrays correlated with expression by RT-PCR ($r = 0.62$, $P = 0.007$). SLFN11 protein expression was assessed by immunoblotting (antibody from Santa Cruz) as previously described (33).

***SLFN11* expression in primary tumors**

Transcriptional profiling was performed on 150 cases of childhood tumors, 50 each of EFT, NB, and RMS (both embryonal and alveolar, in equal numbers) using Affymetrix Human Exon (HuEx) arrays. Data were imported and normalized using PLIER and quantile normalization. Mean expression values were set to 80 per the manufacturer's recommendation. The expression levels for both Schlafen family member 11 (*SLFN11*) and Friend leukemia integration site 1 (*FLI1*) were analyzed for each tumor in each category and compared individually and categorically. Results were expressed as the log to base 10 in each case. For comparison of *SLFN11* versus *FLI1*, a scatter analysis with equal x and y axes (log_{10}) was employed. The R^2 value was calculated using a simple linear regression model to determine the correlation coefficient.

Statistical analysis

Mouse event-free survival (EFS) was graphically represented by the Kaplan–Meier analysis, and EFS between groups was analyzed by the log-rank test using GraphPad Prism (GraphPad Software). EFS was defined as the time from initiating treatment until death, tumor size greater than or equal to 1,500 mm^3, or treatment-related toxicity. For pharmacokinetic experiments, the statistical differences were evaluated by the Student t test. Correlation between rIC_{50} and *SLFN11* expression was determined by Pearson r correlation. The differences in macrophage content in tumors were assessed by the one-way ANOVA. $P < 0.05$ was considered significant.

Results

Antitumor activity of irinotecan or nal-IRI in xenograft models of pediatric cancers

We compared the antitumor activity of nal-IRI (10 mg/kg/dose, total 2 doses: Monday and Thursday) to irinotecan (10 mg/kg/dose, total of 2 doses: Monday and Thursday) in xenograft models (three each) of EFT, RMS, and NB. Treatment with nal-IRI significantly extended EFS compared with control in seven of nine xenograft models and compared with irinotecan in six of nine models (Fig. 1, *P* values are included in Supplementary Table S2).

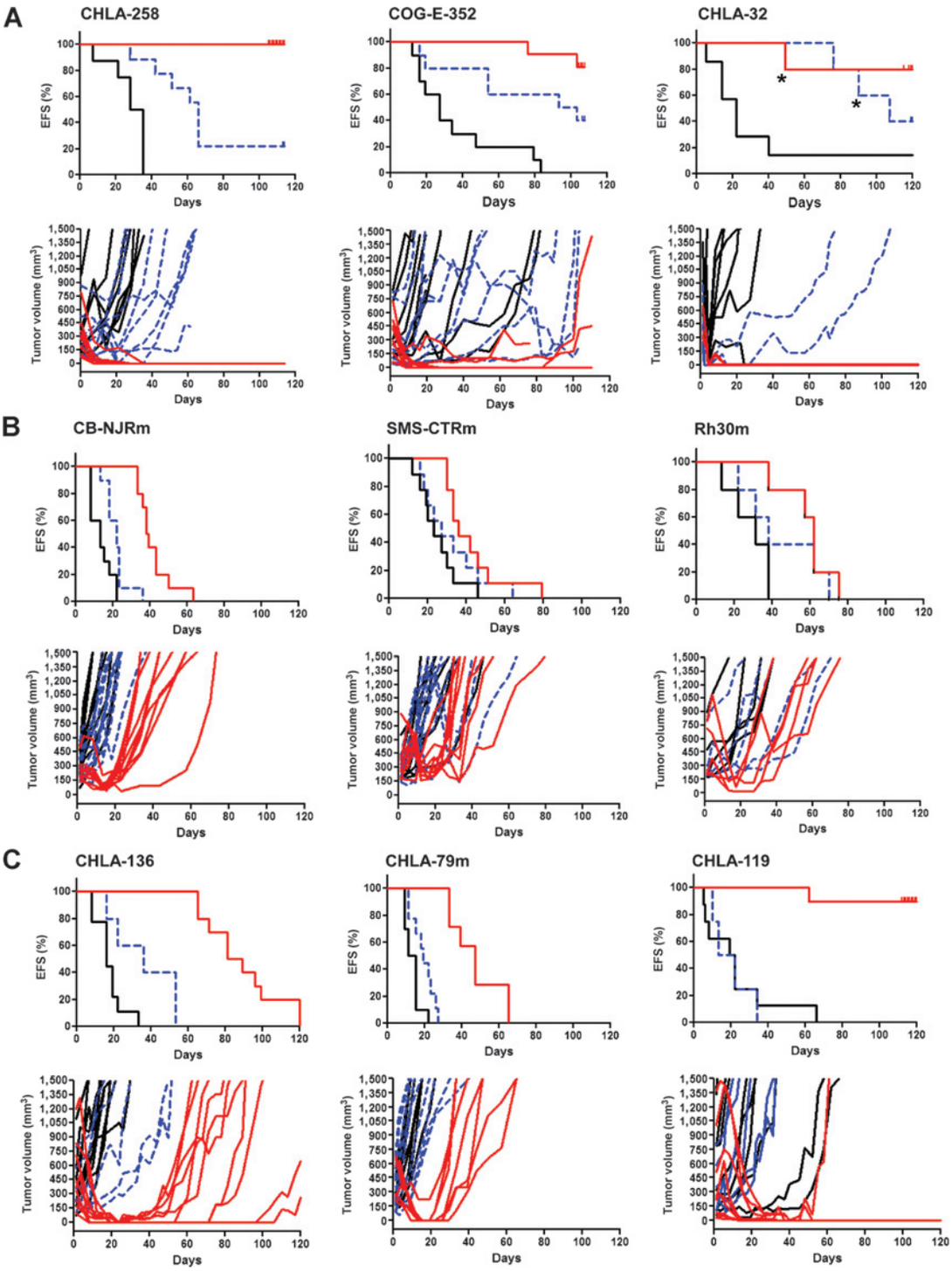

Figure 1.
EFS of tumor-bearing mice. Athymic (nu/nu) mice were engrafted subcutaneously with cell lines from (A) EFT (CHLA-258, COG-E-352, and CHLA-32, (B) RMS (CB-NJRm, SMS-CTRm, and Rh30m, or (C) NB (CHLA-136, CHLA-79m, and CHLA-119). When the average tumor size reached 150 mm^3, the mice were treated with vehicle control (solid black line), 10 mg/kg/d of irinotecan (dotted blue line), or 10 mg/kg/d of nal-IRI (solid red line) in a single injection on day 1 and day 5. Then, the mice were observed for weight changes, diarrhea, or any signs of distress. Mouse EFS (top plot) was quantified as the time taken from the initiation of treatment until the tumor size reached 1,500 mm^3, or for mice to be killed due to treatment-related toxicity. Tumor volume (bottom plot) of individual mice is presented for control (solid black line) versus irinotecan (dotted blue line) nal-IRI (solid red line). Each line represents the percentage of mice remaining event free over time. The number of mice per group, the median EFS, and the *P* values are listed in Supplementary Table S2. *, mice found dead, unknown cause not by tumor progression.

Maintained complete responses were observed over 110 days in the majority of mice treated with nal-IRI, but not free irinotecan, in all EFT xenograft models (CHLA-258, COG-E-352, and CHLA-32). The number of mice per group, the median EFS, and the *P* values are listed in Supplementary Table S2. In one of three RMS mouse models (CB-NJRm), nal-IRI–treated mice showed significantly greater EFS (median survival, 38.5 days) compared with irinotecan (22 days, $P < 0.0001$) or control mice (13 days, $P < 0.0001$). In the three neuroblastoma xenograft models (CHLA-136, CHLA-79m, and CHLA-119), EFS with nal-IRI was greater than with irinotecan ($P < 0.0004$) or vehicle control ($P < 0.0001$), but duration of responses in two of the three NB models was <100 days in the majority of mice treated with nal-IRI. Dosing of 10 mg/kg/d for both nal-IRI and irinotecan was well tolerated in xenografted mice; body weight during the course of therapy is shown for two representative models in Supplementary Fig. S1A. Overall, EFT xenograft mice treated with nal-IRI showed significantly longer EFS relative to RMS or NB (Supplementary Fig. S1B).

We also evaluated nal-IRI alone and when combined with cyclophosphamide when given weekly for 4 weeks in five xenograft models of EFT, including xenografts from cell lines established from progressive disease after myeloablative therapy (CHLA-258 and COG-N-352), compared with three RMS xenograft models. Cyclophosphamide was chosen for the combination studies due to its common use in pediatric oncology, and our data showing that the active metabolite of cyclophosphamide (4-HC) showed the best synergy with topoisomerase I inhibitors among tested agents (34). EFS for all 5 EFT xenograft models treated with nal-IRI + cyclophosphamide was 92% at 150 days, but only 13% at 110 days for the 3 RMS xenografts (Supplementary Fig. S1C). EFS for nal-IRI + cyclophosphamide in RMS xenografts at 80 days was 27% compared with 0% for nal-IRI as a single agent ($P = 0.0014$). However, due to the high activity against EFT of nal-IRI, the increase in EFS for nal-IRI + cyclophosphamide of 92% compared with 73% for nal-IRI alone was not significant ($P = 0.08$).

Plasma and tissue pharmacokinetics in nontumor-bearing mice

Plasma and tissue pharmacokinetic profiles for irinotecan and SN-38 following the administration of free irinotecan or nal-IRI at 5, 10, and 20 mg/kg in nontumor-bearing BALB/c mice are shown in Fig. 2A. After a 20 mg/kg dose of free irinotecan, the observed maximum plasma concentration of irinotecan was 2.8 ± 0.3 μg/mL at 5 minutes after injection, whereas nal-IRI at the same dose achieved 197.0 ± 10.3 μg/mL at 1 hour ($P < 0.01$). At 8 hours after injection with free irinotecan, the irinotecan concentration was <0.01 μg/mL, whereas it was 98.0 ± 12.7 μg/mL at 8 hours after nal-IRI injection ($P < 0.01$). The rapid clearance of SN-38 from mouse blood following free irinotecan administration was consistent with the observed irinotecan clearance. The plasma concentration of SN-38 after injection of nal-IRI showed an increase up to 12 hours after injection followed by a gradual decrease over time. The pharmacokinetic parameters in mice for both formulations are summarized in Supplementary Table S3. The half-life of irinotecan (0.8–1.1 hours) in plasma was significantly shorter than that of nal-IRI (2.6–4.4 hours, $P = 0.001$), and the clearance was greater with irinotecan (138–300 mL/h) compared with nal-IRI (0.2–0.4 mL/h, $P = 0.024$).

After the administration of irinotecan we observed a concentration drop to 1/20–1/300 of the maximum concentrations over 8 hours in all tissues (Fig. 2B). Irinotecan and SN-38 levels were higher in liver, spleen, and kidney relative to the lung and brain. Irinotecan and SN-38 concentrations achieved by nal-IRI were comparable with free irinotecan soon after intravenous injection, but elimination of both irinotecan and SN-38 from tissues was substantially slower for nal-IRI than for free irinotecan (Fig. 2C).

Biodistribution in tumor-bearing mice

In nu/nu mice bearing human NB xenografts (CHLA-136), intravenous injection of 20 mg/kg free irinotecan achieved a irinotecan plasma level of 0.06 ± 0.01 μg/mL at 4 hours after injection, barely detectable above the limit of quantitation at 24 hours (Fig. 3A, left). At the same dose, nal-IRI showed plasma irinotecan concentrations at 4 hours (131.4 ± 35.8 μg/mL) 1,000-fold higher than achieved with free irinotecan. Irinotecan was above the detection limit (0.014 ± 0.005 μg/mL) 48 hours after nal-IRI injection. Plasma SN-38 concentrations were >100-fold higher with nal-IRI relative to irinotecan (Fig. 3A, right).

Elimination of irinotecan and SN-38 for most tissues was more rapid with free irinotecan relative to nal-IRI in tumor-bearing nu/nu mice (Fig. 3B–F), similar to what was observed in nontumor-bearing mice. At 48 hours after injecting free irinotecan, the irinotecan levels in tissues and tumor were decreased by 2 orders of magnitude compared with those at 4 hours, and the concentration in the brain was below the detection limit (Fig. 3B). Elimination of nal-IRI in tissues and tumor was considerably slower than observed for irinotecan (Fig. 3B–F). After 4 hours of nal-IRI injection, the tissue levels of irinotecan and SN-38 in the liver reached 548 ± 396 μg/g protein (irinotecan) and 15.1 ± 8.6 μg/g protein (SN-38), which are the highest in all tissues measured (Fig. 3E). The levels of SN-38 in tumor at 48 hours with nal-IRI were almost 10-fold higher than we observed with irinotecan (Fig. 3F).

In vitro conversion of irinotecan to SN-38

As liposomal stabilization of irinotecan should minimize release of the drug before it reaches tumor sites, we did not expect to see >100-fold higher plasma SN-38 levels in nal-IRI–injected mice compared with free irinotecan-injected mice (Fig. 3A). As nal-IRI–injected mice did not experience greater systemic toxicities relative to irinotecan-injected mice, it was speculated that higher SN-38 concentrations might have resulted after samples were collected. Thus, we assessed two methods of blood sample collection, direct extraction without freezing plasma samples versus freezing samples for future analyses. Freezing samples for future analyses resulted in approximately 2-fold higher SN-38 concentrations up to 20 hours after the injection of nal-IRI (Supplementary Fig. S2A and S2B), indicating that irinotecan is further converted to SN-38 during the freeze-thaw process by carboxylesterase in mouse plasma.

A plasma carboxylesterase content is higher in mice than in humans (35), and postcollection conversion of irinotecan to SN-38 may be less of an issue in humans. Indeed, *in vitro* enzyme kinetic experiments demonstrated more limited conversion of irinotecan to SN-38 for human versus mouse plasma at 24 hours (37°C). The Michaelis–Menten kinetic parameters of V_{max} (maximum velocity) and K_m (substrate concentration that yield a half-maximal velocity) were 0.3 pmol/hr/mg protein and 12,471 ng/mL (31.8 μmol/L) in human plasma, and 1.3 pmol/hr/mg

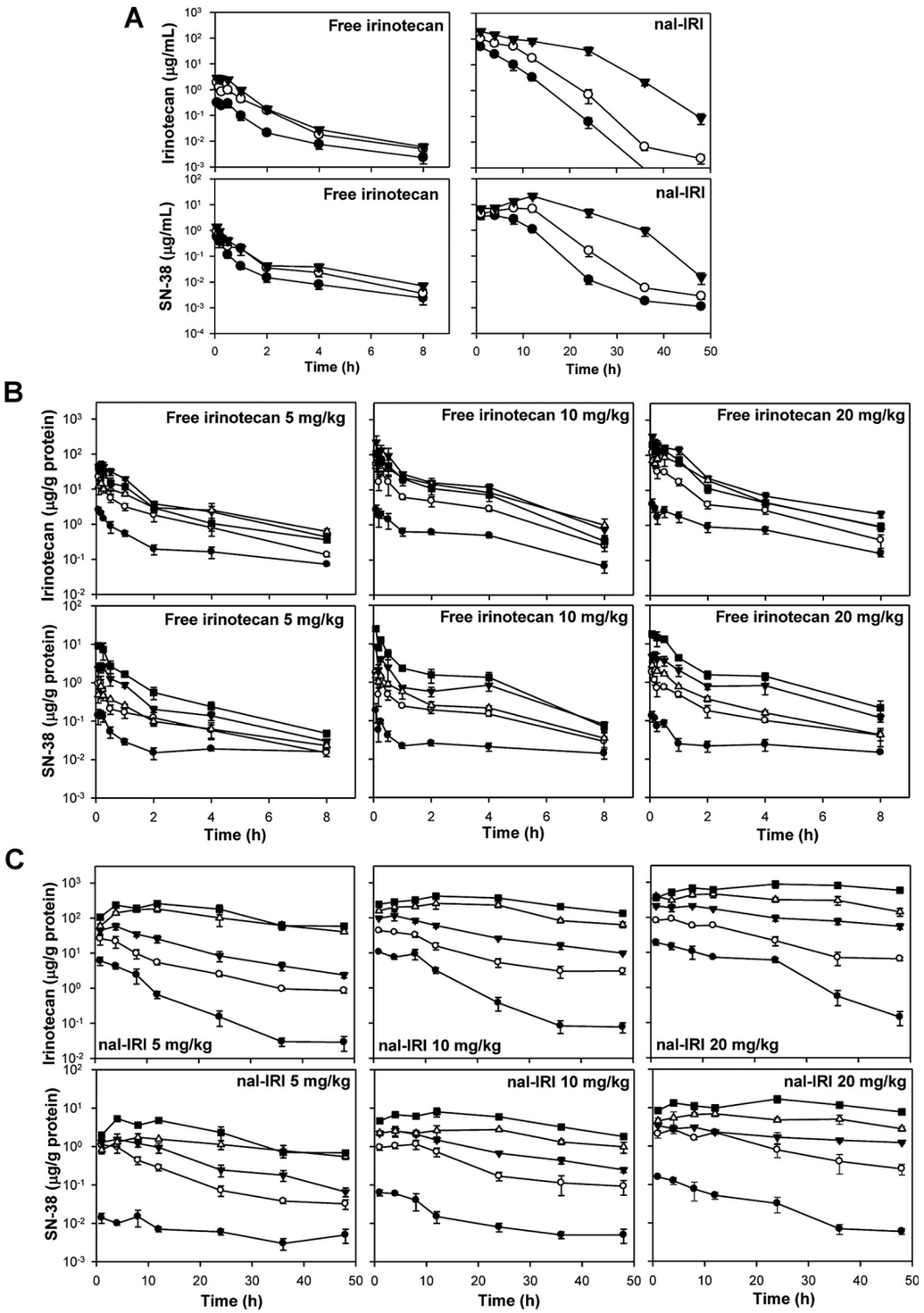

Figure 2.
Plasma and tissue pharmacokinetic profiles for irinotecan and SN-38 following single doses of irinotecan or nal-IRI. A, concentration of irinotecan (top plot) and SN-38 (bottom plot) as a function of time after irinotecan (left) or nal-IRI (right) injection. Female BALB/c mice were injected intravenously with a single dose of 5 mg/kg (●), 10 mg/kg (○), or 20 mg/kg (■) of drug solution. Blood samples were collected by cardiac puncture at various time points: 5, 10, 15, and 30 minutes, 1, 2, 4, and 8 hours for irinotecan; 1, 4, 8, 12, 24, 36, and 48 hours for nal-IRI. Points, mean; bars, ± SE ($n = 3$). B and C, tissue elimination profiles for irinotecan and SN-38 following three single doses of irinotecan (B) or nal-IRI (C). Female BALB/c mice were injected intravenously with 5, 10, or 20 mg/kg dose of drug solution. Mouse tissues include brain (●), lung (○), kidney (▼), spleen (△), and liver (■). Concentrations detected below the lower limit of quantification were not shown. Points, mean; bars, ± SE ($n = 3$).

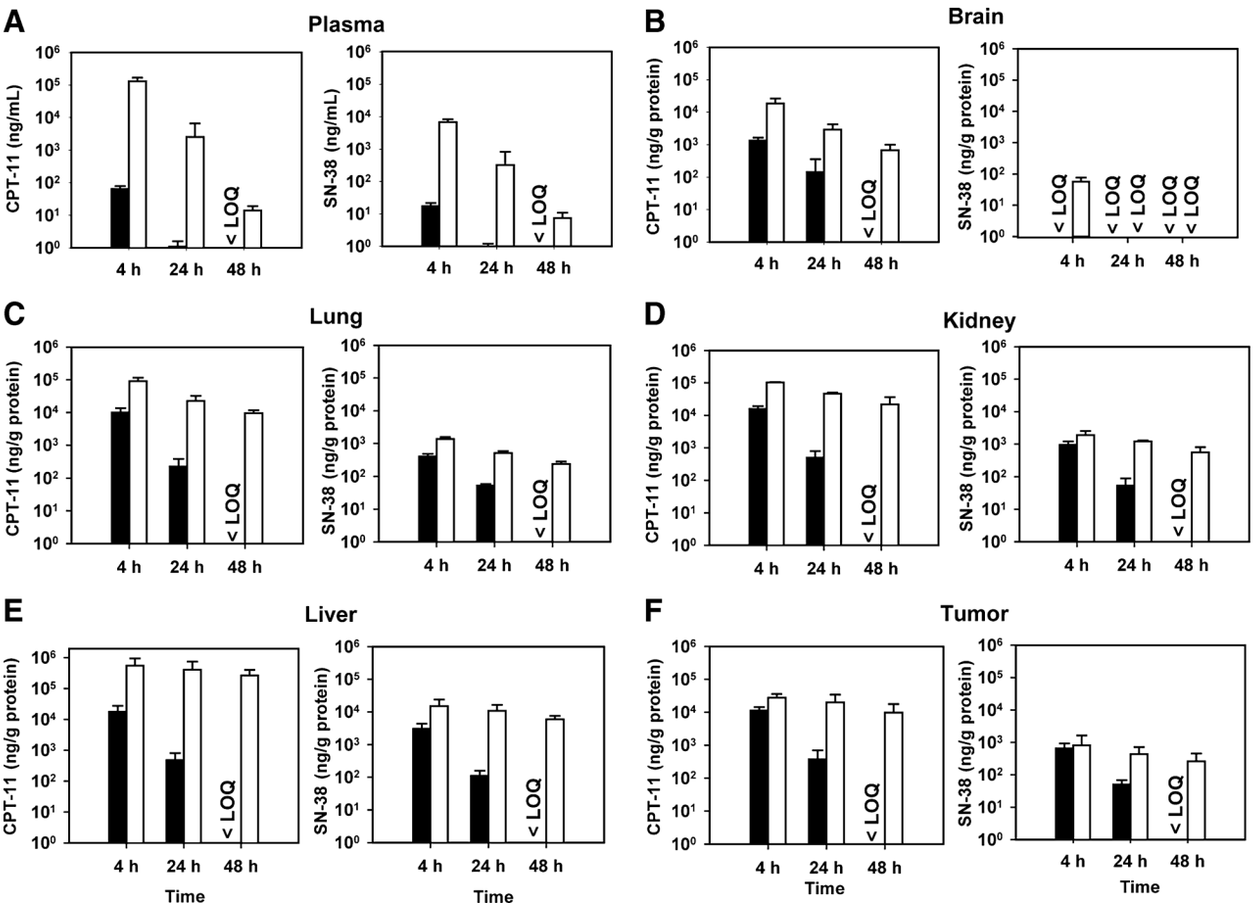

Figure 3.
Plasma and tissue/tumor concentrations for irinotecan and SN-38 following a single dose of irinotecan or nal-IRI in nu/nu mice. Female nu/nu mice bearing subcutaneous human neuroblastoma xenografts (CHLA-136) were injected intravenously with a single dose of 20 mg/kg of drug solution. A, the plasma concentrations of irinotecan (left) and SN-38 (right) were measured at 4, 24, and 48 hours after a single intravenous injection of irinotecan or nal-IRI. B–E, the tissue concentrations of irinotecan (left) and SN-38 (right) were measured at 4, 24, and 48 hours after a single intravenous injection of irinotecan or nal-IRI. F, the intratumoral concentrations of irinotecan and SN-38 were assessed at 4, 24, and 48 hours after a single intravenous injection of irinotecan or nal-IRI. Points, mean; bars, ± SE ($n = 3$). Black bars, irinotecan; white bars, nal-IRI. <LOQ, the detected concentration was below the lower limit of quantification.

protein and 393 ng/mL (1.0 μmol/L) in mouse plasma (Supplementary Fig. S2C).

Macrophage infiltration and tumor pharmacokinetics (PK) after nal-IRI treatment

Responses to nal-IRI in xenograft models varied widely, with activity in EFT being consistently greater than what was observed for RMS or NB xenografts (Fig. 1 and Supplementary Fig. S1B). Tumor-associated macrophages could potentially concentrate nal-IRI and facilitate release of the more potent SN-38 into tumors. However, we observed no significant differences in macrophage infiltration among NB, RMS, or EFT tumor xenografts at 0, 48, or 168 hours following nal-IRI treatment (Fig. 4A, $P = 0.31$, representative pictures in Supplementary Fig. S3). Treatment with nal-IRI significantly increased macrophage infiltration in all three models ($P < 0.005$), but no greater infiltration was seen in any specific tumor type relative to other models at 168 hours after the treatment (Fig. 4A, $P = 0.37$).

The tumor concentrations of irinotecan (but not of SN-38) in EFT or RMS xenografts were significantly higher than NB xenografts (Fig. 4B, $P < 0.05$). Plasma concentrations of irinotecan and SN-38 at 48 hours after injection in RMS xenograft mice were apparently lower compared with NB or EFT xenograft mice, although the differences were not statistically significant ($P = 0.07$). However, SN-38 plasma concentrations were above the detection limit (2.5 ng/mL) at 168 hours in the RMS model, whereas NB or EFT models were below the limit of detection. Given that no differences in macrophage infiltration were seen for the 3 tumor types, and that the tumor concentrations of the drug and the metabolite were not higher in EFT models (which showed durable complete responses in all five models tested, Fig. 1 and Supplementary Fig. S1B and S1C), macrophage infiltration or tumor concentrations of irinotecan or SN-38 were excluded as the major mechanism for the remarkably high nal-IRI activity observed in EFT relative to NB or RMS xenografts.

SLFN11 expression in association with sensitivity to SN-38

High expression of the putative DNA/RNA helicase *SLFN11* has been recently reported to correlate with sensitivity to DNA

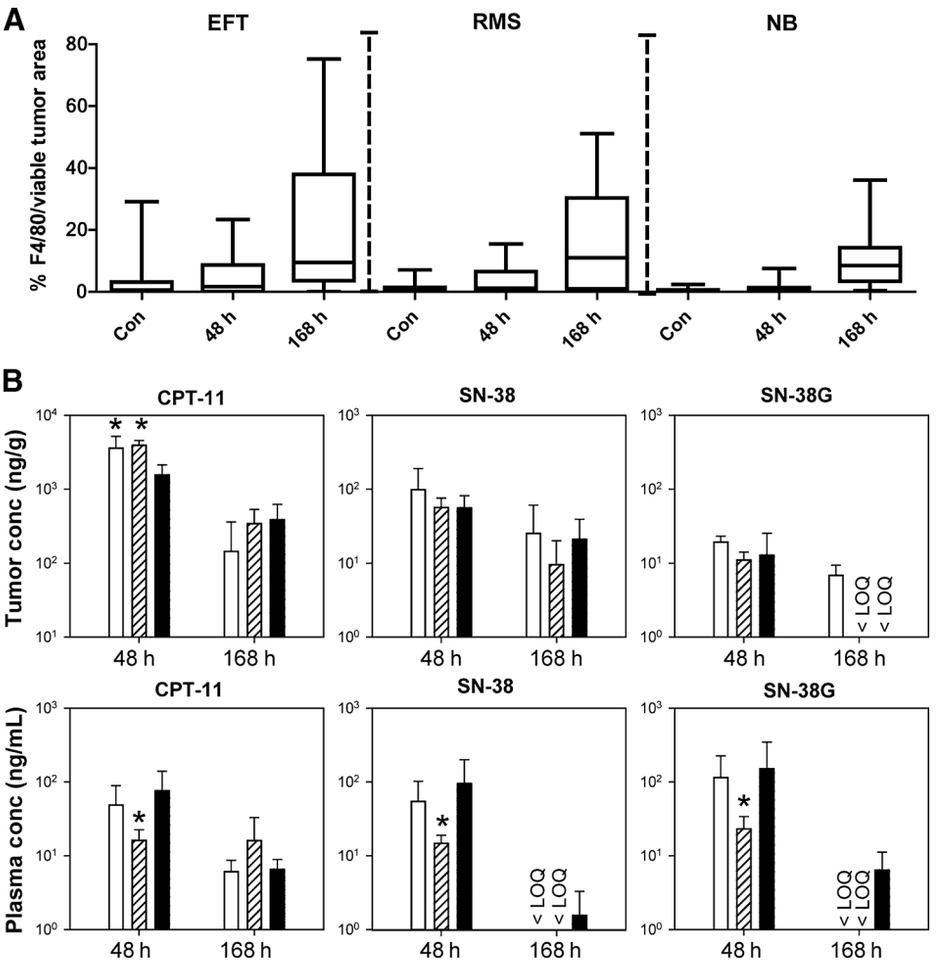

Figure 4.
Macrophage infiltration in pediatric tumors after nal-IRI treatment. Tumors from mice xenografted with EFT (CHLA-258), RMS (CB-NJRm), or NB (CHLA-79) were collected 48 and 168 hours after treatment with 10 mg/kg/d of nal-IRI. The tumors were snap-frozen for macrophage infiltration assays (A) and for PK analyses (B). A, macrophage infiltration was assessed as described in Materials and Methods; data are the % F4/80 staining cells per viable tumor area. A minimum of 5 fields were evaluated for macrophage content, and each time point has 3 or more mice. Differences in macrophage content by tumor type were not significant ($P = 0.37$ at 168 hours), but for all 3 tumor types macrophage infiltration was significantly ($P < 0.005$) increased by nal-IRI treatment. B, blood was collected 48 and 168 hours after treatment by cardiac puncture. Plasma samples were stored in −80 °C until analyses. White bar, EFT; hatched bar, RMS; solid bar, NB. SN-38G, SN-38 glucuronide. *, statistically significant difference ($P < 0.05$). <LOQ, below the limit of detection (2.5 ng/mL).

damaging agents (20, 21). We observed that sensitivity to DNA damaging agents (4-HC: active metabolite of cyclophosphamide, topotecan, SN-38), as determined by the DIMSCAN cytotoxicity assay, showed a significant correlation with *SLFN11* expression assessed by the Affymetrix Human Exon Array in 17 EFT cell lines [Supplementary Fig. S4, $P < 0.005$ for all three drugs, $r = -0.95$ (4-HC), -0.76 (topotecan), -0.84 (SN-38)]. Using quantitative RT-PCR for 20 EFT, 20 NB, and 12 RMS cell lines, we observed that *SLFN11* expression was >100-fold higher in EFT relative to NB cell lines, whereas the expression varied widely in RMS (Fig. 5A). SLFN11 protein and mRNA expression were consistent, showing higher expression in the majority of EFT cell lines relative to NB or RMS (Fig. 5B). We observed an inverse correlation between *SLFN11* mRNA expression measured by RT-PCR and the relative inhibitory/cytotoxic concentrations (rIC_{50}) concentrations (measured by DIMSCAN) of SN-38 for 20 EFT cell lines ($P = 0.004$, $r = -0.63$, Fig. 5C). However, no significant correlation between rIC_{50} and *SLFN11* mRNA expression was observed in RMS or NB cell lines. ($P = 0.26$ and $P = 0.21$; Fig. 5D and E).

As *SLFN11* mRNA expression assessed by RT-PCR and Affymetrix HuEx microarray correlated well in cell lines ($r = 0.62$, $P = 0.007$), we examined *SLFN11* mRNA expression data from HuEx microarrays for primary tumors (50 each for EFT, RMS, and NB). Of the 50 EFT samples, 90% had the EWS–FLI1 translocation and 10% had EWS–ERG. Rhadomyosarcomas were 1/3rd alveolar and 2/3rds embryonal and neuroblastomas were 1/3rd favorable biology, 1/3rd *MYCN*-amplified, and 1/3rd MYCN-nonamplified with unfavorable histopathology. Consistent with the expression in the cell line panels, median *SLFN11* mRNA expression was approximately 10-fold higher in EFT primary tumors compared with NB or RMS primary tumors ($P < 0.0001$; Fig. 6A). FLI1 is not normally expressed, and thus using the 3′end of the gene provides a surrogate for the chimeric EWS–FLI1 gene. Using this approach, coexpression of FLI1 and *SLFN11* was evaluated using the same microarray data employed for Fig. 6A, comparing an exon of *SLFN11* (3753518) with the 8th exon of *FLI1* (3355784), which is expressed at high levels only when translocated, as part of EWS–FLI1 ($r = 0.51$, $P < 0.001$; Fig. 6B).

Discussion

Although diarrhea is the dose-limiting toxicity of irinotecan, it can be managed to some degree by employing antidiarrhea medications at the early stage of treatment (14). Other limitations of irinotecan for its clinical application include (i) poor pharmacokinetic properties only allowing short tumor exposure to the

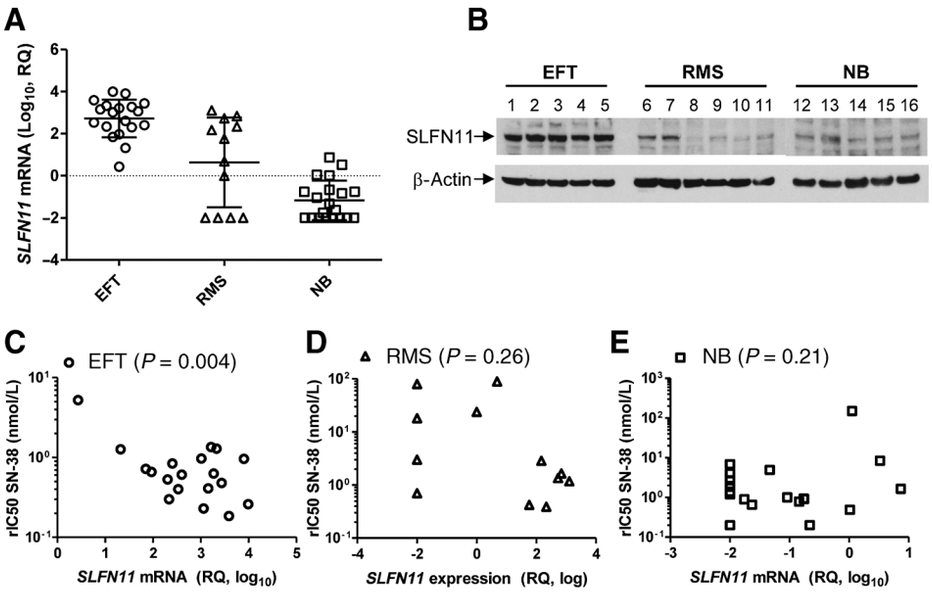

Figure 5.
Correlation between *SLFN11* expression and sensitivity to SN-38 in pediatric solid tumor cell lines. Cytotoxicity of SN-38 was evaluated, and mRNA was isolated from 20 NB, 12 RMS, and 20 EFT cell lines (see Supplementary Table S1 for cell line characteristics). A, *SLFN11* mRNA expression in panels of NB, RMS, and EFT cell lines. *SLFN11* mRNA expression was compared among the three histotypes of pediatric cancers using quantitative RT-PCR. The data were expressed in relative quantitation (RQ) using the BIRCH cell line (RMS) as the standard (marked as 0 on the *Y* axis). Each data point represents an average of 3 biologic replicates measured in three technical replicates. B, SLFN11 protein expression in NB, RMS, and EFT cell lines assessed by immunoblotting. Lanes 1–5 (EFT), from left, CHLA-32, CHLA-258, TC-32, TC-72, CHLA-9; Lanes 6–11 (RMS), from left, TTC-442, Rh30, Rh18, RD, BIRCH, Rh41; Lanes 12–16 (NB), from left, CHLA-144, SK-N-BE(1), CHLA-90, CHLA-136, SMS-KCN. EFT cell lines were used in both experiments to compare the protein expression levels in NB and RMS relative to EFT cell lines. C–E, correlation between *SLFN11* mRNA expression and SN-38 cytotoxicity in EFT (C), RMS (D), and NB (E) cell lines. The rIC_{50} of SN-38 was correlated with *SLFN11* expression in EFT ($r = -0.63$), NB ($r = 0.31$), and RMS ($r = -0.31$) cell lines by Pearson *r* correlation. rIC_{50} was determined using GraphPad Prism from survival fractions of cells after treating them with 9 different concentrations of SN-38 in 3-fold increments. Each concentration had 6 replicates.

drug and its active metabolite (SN-38) and (ii) hydrolysis of active lactone rings in irinotecan and SN-38 to inactive carboxylate forms in neutral to basic pH (36). Stable liposomal encapsulation of irinotecan may minimize the transformation of the irinotecan into its inactive carboxylate form by reducing the direct exposure of the drug to physiologic pH and prolong the residence time of active drug and metabolites in the system. Because only the lactone form of camptothecin analogues is able to transverse cellular membranes (37), decreasing hydrolysis of irinotecan by encapsulating in liposomes has the potential to improve clinical activity.

Recent advances in intraliposomal encapsulation technology showed that irinotecan formulated as a nanoliposomal formulation (nal-IRI = MM-398) achieved high *in vivo* chemical stability, liposome retention, and improved residence time of irinotecan in rats (13). We observed that levels of SN-38 in xenografted tumors were significantly higher with nal-IRI than with irinotecan. The increased tumor exposure to irinotecan and SN-38 achieved with nal-IRI relative to irinotecan was consistent with the higher antitumor activity and superior EFS seen in the mouse xenograft models of pediatric solid tumors treated with nal-IRI compared with irinotecan in the majority of xenograft models tested.

The accumulation of liposomal drugs in tumors is suggested to occur via two pathways. One is via the enhanced permeability and retention (EPR) effect (11, 38). Liposomes do not readily diffuse out of the blood vessels in healthy tissues (39), but the leaky vasculature and impaired lymphatic drainage in tumor can facilitate the spontaneous accumulation of liposomes in these areas (40). The other pathway is through the localization of liposomes to mononuclear phagocytes such as macrophages (38). Although the number of macrophages varied greatly among different tumors, the percentage of tumor-associated macrophages is usually maintained at a stable level for a particular tumor type (41). In addition, macrophage carboxylesterases in tumor is a presumed mechanism for the conversion of irinotecan to SN-38 in human tumors (14, 42, 43), and the macrophage levels in nu/nu mice are comparable with levels observed in immunocompetent mice (44). However, we observed that neither macrophage infiltration nor intratumoral concentrations of irinotecan or SN-38 were significantly higher in EFT models in which durable responses to nal-IRI were seen relative to xenografts of NB and RMS that were less responsive to nal-IRI. Our data showed that macrophage infiltration into tumors or tumor pharmacokinetics does not vary among xenografts of the 3 histotypes of pediatric solid tumors that we tested, and thus is unlikely to be the reason for the consistently high responsiveness of EFT xenografts to nal-IRI relative to other histotypes.

The mRNA expression of *SLFN11*, a putative RNA/DNA helicase, has been reported to correlate with the sensitivity to DNA damaging agents in the NCI60 panel of cell lines (21) or with the sensitivity to irinotecan in three EFT cell lines (20). Consistent with the previous report by Barretina and colleagues showing highest expression of *SLFN11* in EFT primary samples among various cancer types (20), we found that *SLFN11* mRNA expression was significantly higher (>100-fold) in EFT cell lines relative

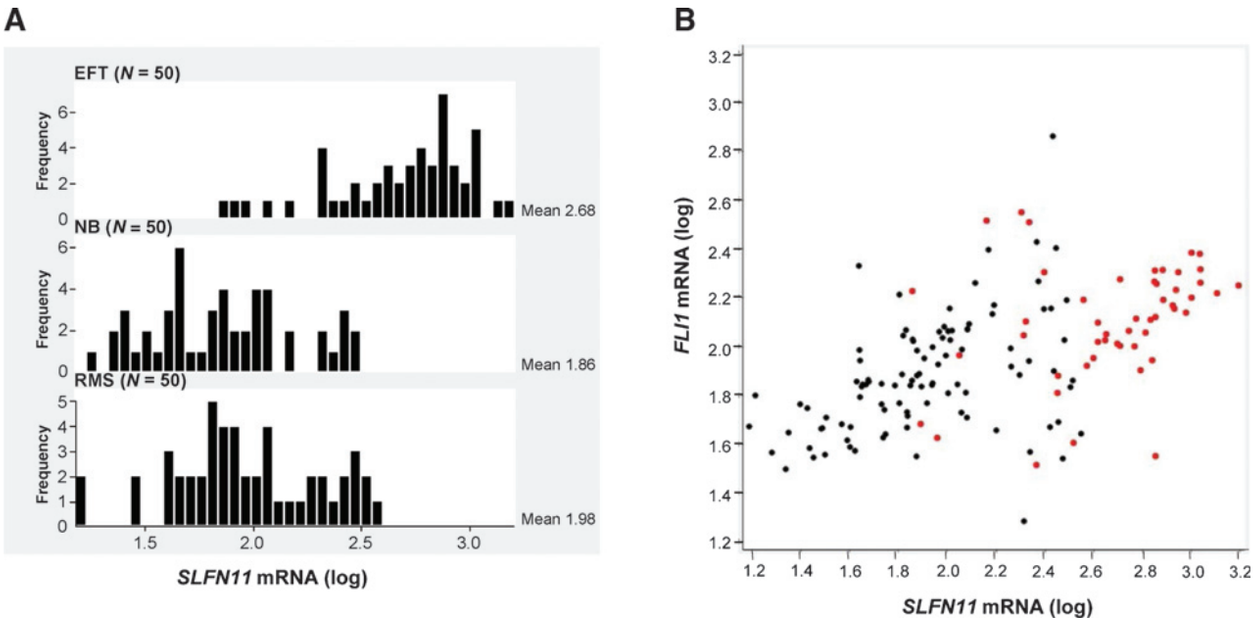

Figure 6.
SLFN11 expression in primary patient samples. A, histograms of *SLFN11* expression (measured using Affymetrix Exon arrays) for 50 primary tumors each of EFT, RMS, and NB. Data are displayed on a $\log_{10}$ scale, with mean log expression values for each. B, using the same samples as shown in Fig. 6A, we observed a significant correlation ($P < 0.001$) between *SLFN11* expression and *FLI1* expression (measured using Affymetrix Exon arrays) in EFT, RMS, and NB tumors ($r = 0.51$). As shown in Fig. 6A, *SLFN11* is highly expressed in EFT; virtually all the high expressers for both *SLFN11* and *FLI1* are EFT, suggesting a functional link between expression of the two genes. EFT samples are shown as red dots.

to NB and RMS cell lines (Fig. 5). Although NB cell lines exhibit much lower *SLFN11* expression, the sensitivity to SN-38 in NB cell lines was similar to that in EFT cell lines, suggesting that *SLFN11* expression is not the primary driver of SN-38 sensitivity across all histotypes. For example, CHLA-119 (established at time of relapse after intensive consolidation chemotherapy; CCG-3891) that included topoisomerase II but not a topoisomerase I inhibitor is one of four NB cell lines with the lowest *SLFN11* expression, but nine of the ten xenograft mice survived >120 days after two doses of nal-IRI (Fig. 1).

In 20 EFT cell lines, we observed a strong correlation between *SLFN11* expression and SN-38 sensitivity that was confirmed by both microarray and quantitative RT-PCR experiments. The high sensitivity of EFT cell lines to SN-38 *in vitro* was consistent with *in vivo* EFT tumor xenograft responses to nal-IRI. Thus, the high activity seen for nal-IRI in EFT xenografts is likely due to the improved pharmacokinetic properties of nal-IRI enhancing exposure to SN-38 in the tumor combined with the high sensitivity to SN-38 associated with high *SLFN11* expression.

We observed significantly higher expression of *SLFN11* mRNA in primary tumors from EFT relative to RMS and NB, which is consistent with our cell line data and with the xenograft response data, suggesting that clinically EFT may be particularly sensitive to nal-IRI. *EWS/FLI* is thought to be an aberrant transcription factor that is specifically expressed in EFT (22). *FLI1* is normally not expressed in EFT or other childhood tumors, other than as a partner of EWS (which is ubiquitously expressed in most tissues) to form the *EWS–FLI1* chimeric gene found in 85% to 95% of Ewing's sarcomas. Thus, we examined the correlation between expression of *FLI1* (which on Affymetrix microarrays provides a surrogate for *EWS/FLI* expression) and *SLFN11*. We observed a strong correlation between *SLFN11* and *FLI1* mRNA expression, and *SLFN11* may be a direct target of *EWSR1–FLI1* as evidenced by ChipSeq analysis data from Kauer and colleagues (45). The relationship of *SLFN11* expression to sensitivity of tumors to nal-IRI will ultimately need to be addressed in clinical trials, and the mechanism by which *SLFN11* expression confers sensitivity to SN-38 will need to be explored in further laboratory studies.

Clinical trials of nal-IRI in patients with metastatic colorectal cancer and pancreatic cancer are ongoing (ref. 46; clinicaltrials.gov ID: NCT01494506, NCT01375816), with positive results being recently reported for nal-IRI in a pivotal phase III study of pancreatic cancer (19) Based on published data and data from the present study, evaluations of *SLFN11* as a potential biomarker for nal-IRI activity are planned. Our study is the first to show that nal-IRI has substantially improved antitumor activity over irinotecan in xenograft models of pediatric cancers. The striking antitumor activity in EFT xenografts seen with nal-IRI was likely due to the combination of the advantageous pharmacokinetic properties of nal-IRI combined with the high sensitivity to SN-38 of EFT, which was significantly correlated with *SLFN11* expression. Based on the preclinical studies reported here, a phase I study of nal-IRI combined with cyclophosphamide in pediatric solid tumors (SPOC 2012-001;NCT 02013336) is under way in the South Plains Oncology Consortium (www.SPONC.org).

Disclosure of Potential Conflicts of Interest

J.B. Fitzgerald has ownership interest (including patents) in Merrimack Pharmaceuticals. D.C. Drummond is employed by and has ownership interest (including patents) in Merrimack Pharmaceuticals. No potential conflicts of interest were disclosed by the other authors.

Authors' Contributions

Conception and design: M.H. Kang, J.B. Fitzgerald, D.C. Drummond, C.P. Reynolds

Development of methodology: M.H. Kang, J. Wang, M.R. Makena, N. Paz, C.P. Reynolds

Acquisition of data (provided animals, acquired and managed patients, provided facilities, etc.): M.H. Kang, J. Wang, M.R. Makena, J.-S. Lee, N. Paz, C.P. Hall, M.M. Song, R.I. Calderon, R.E. Cruz, A. Hindle, W. Ko, C.P. Reynolds

Analysis and interpretation of data (e.g., statistical analysis, biostatistics, computational analysis): M.H. Kang, J. Wang, M.R. Makena, C.P. Hall, W. Ko, J.B. Fitzgerald, T.J. Triche, C.P. Reynolds

Writing, review, and/or revision of the manuscript: M.H. Kang, J. Wang, C.P. Hall, J.B. Fitzgerald, D.C. Drummond, C.P. Reynolds

Administrative, technical, or material support (i.e., reporting or organizing data, constructing databases): M.H. Kang, M.R. Makena, R.E. Cruz

Study supervision: M.H. Kang, D.C. Drummond, C.P. Reynolds

Acknowledgments

The authors thank Annie Chung, Srirupa Cheerla, Dr. Rupeng Zhou, and Dr. Yongku Ryu for their technical support.

Grant Support

This work was supported by Rett's Initiative (www.EFTlab.org) of the Nearburg Foundation via CureSearch National Childhood Cancer Foundation, The Chris Carrey Foundation, and by National Cancer Institute grant CA82830.

The costs of publication of this article were defrayed in part by the payment of page charges. This article must therefore be hereby marked *advertisement* in accordance with 18 U.S.C. Section 1734 solely to indicate this fact.

Received July 21, 2014; revised November 20, 2014; accepted November 23, 2014; published online March 2, 2015.

References

1. Sawada S, Okajima S, Aiyama R, Nokata K, Furuta T, Yokokura T, et al. Synthesis and antitumor activity of 20(S)-camptothecin derivatives: carbamate-linked, water-soluble derivatives of 7-ethyl-10-hydroxycamptothecin. Chem Pharm Bull (Tokyo) 1991;39:1446–50.
2. Saltz LB, Cox JV, Blanke C, Rosen LS, Fehrenbacher L, Moore MJ, et al. Irinotecan plus fluorouracil and leucovorin for metastatic colorectal cancer. N Engl J Med 2000;343:905–14.
3. Houghton JA, Cheshire PJ, Hallman JD 2nd, Lutz L, Luo X, Li Y, et al. Evaluation of irinotecan in combination with 5-fluorouracil or etoposide in xenograft models of colon adenocarcinoma and rhabdomyosarcoma. Clin Cancer Res 1996;2:107–18.
4. Rivory LP, Robert J. Molecular, cellular, and clinical aspects of the pharmacology of 20(S)camptothecin and its derivatives. Pharmacol Ther 1995;68:269–96.
5. Kawato Y, Aonuma M, Hirota Y, Kuga H, Sato K. Intracellular roles of SN-38, a metabolite of the camptothecin derivative CPT-11, in the antitumor effect of CPT-11. Cancer Res 1991;51:4187–91.
6. Chabot GG. Clinical pharmacokinetics of irinotecan. Clin Pharmacokinet 1997;33:245–59.
7. Messerer CL, Ramsay EC, Waterhouse D, Ng R, Simms EM, Harasym N, et al. Liposomal irinotecan: formulation development and therapeutic assessment in murine xenograft models of colorectal cancer. Clin Cancer Res 2004;10:6638–49.
8. Stewart CF, Zamboni WC, Crom WR, Houghton PJ. Disposition of irinotecan and SN-38 following oral and intravenous irinotecan dosing in mice. Cancer Chemother Pharmacol 1997;40:259–65.
9. Rowinsky EK, Grochow LB, Ettinger DS, Sartorius SE, Lubejko BG, Chen TL, et al. Phase-I and pharmacological study of the novel topoisomerase-I inhibitor 7-Ethyl-10-[4-(1-Piperidino)-1-Piperidino]Carbonyloxycamptothecin (Cpt-11) administered as A 90-minute infusion every 3 weeks. Cancer Res 1994;54:427–36.
10. Kehrer DF, Sparreboom A, Verweij J, de Bruijn P, Nierop CA, van de Schraaf J, et al. Modulation of irinotecan-induced diarrhea by cotreatment with neomycin in cancer patients. Clin Cancer Res 2001;7:1136–41.
11. Drummond DC, Meyer O, Hong KL, Kirpotin DB, Papahadjopoulos D. Optimizing liposomes for delivery of chemotherapeutic agents to solid tumors. Pharmacol Rev 1999;51:691–743.
12. Sadzuka Y, Hirotsu S, Hirota S. Effect of liposomalization on the antitumor activity, side-effects and tissue distribution of CPT-11. Cancer Lett 1998;127:99–106.
13. Drummond DC, Noble CO, Guo ZX, Hong K, Park JW, Kirpotin DB. Development of a highly active nanoliposomal irinotecan using a novel intraliposomal stabilization strategy. Cancer Res 2006;66:3271–7.
14. Noble CO, Krauze MT, Drummond DC, Yamashita Y, Saito R, Berger MS, et al. Novel nanoliposomal CPT-11 infused by convection-enhanced delivery in intracranial tumors: pharmacology and efficacy. Cancer Res 2006;66:2801–6.
15. Dickinson PJ, LeCouteur RA, Higgins RJ, Bringas JR, Roberts B, Larson RF, et al. Canine model of convection-enhanced delivery of liposomes containing CPT-11 monitored with real-time magnetic resonance imaging. J Neurosurg 2008;108:989–98.
16. Krauze MT, Noble CO, Kawaguchi T, Drummond D, Kirpotin DB, Yamashita Y, et al. Convection-enhanced delivery of nanoliposomal CPT-11 (irinotecan) and PEGylated liposomal doxorubicin (Doxil) in rodent intracranial brain tumor xenografts. Neuro Oncol 2007;9:393–403.
17. Roy AC, Park SR, Cunningham D, Kang YK, Chao Y, Chen LT, et al. A randomized phase II study of PEP02 (MM-398), irinotecan or docetaxel as a second-line therapy in patients with locally advanced or metastatic gastric or gastro-oesophageal junction adenocarcinoma. Ann Oncol 2013;24:1567–73.
18. Ko AH, Tempero MA, Shan YS, Su WC, Lin YL, Dito E, et al. A multinational phase 2 study of nanoliposomal irinotecan sucrosofate (PEP02, MM-398) for patients with gemcitabine-refractory metastatic pancreatic cancer. Br J Cancer 2013;109:920–5.
19. Von Hoff D, Li CP, Wang-Gillam A, Bodoky G, Dean A, Jameson G, et al. NAPOLI-1: randomized phase 3 study of MM-398 (nal-IRI), with or without 5-fluorouracil and leucovorin, versus 5-fluorouracil and leucovorin, in metastatic pancreatic cancer progressed on or following gemcitabine-based therapy. Ann Oncol 2014;25:ii105–ii106.
20. Barretina J, Caponigro G, Stransky N, Venkatesan K, Margolin AA, Kim S, et al. The cancer cell line encyclopedia enables predictive modelling of anticancer drug sensitivity. Nature 2012;483:603–7.
21. Zoppoli G, Regairaz M, Leo E, Reinhold WC, Varma S, Ballestrero A, et al. Putative DNA/RNA helicase Schlafen-11 (SLFN11) sensitizes cancer cells to DNA-damaging agents. Proc Natl Acad Sci U S A 2012;109:15030–5.
22. Owen LA, Lessnick SL. Identification of target genes in their native cellular context: an analysis of EWS/FLI in Ewing's sarcoma. Cell Cycle 2006;5:2049–53.
23. Masters JR, Thomson JA, Daly-Burns B, Reid YA, Dirks WG, Packer P, et al. Short tandem repeat profiling provides an international reference standard for human cell lines. Proc Natl Acad Sci U S A 2001;98:8012–7.
24. Stoscheck CM. [6] Quantitation of protein. In:Murray PD, editor. Methods in enzymology: guide to protein purification. Volume 182 ed. Waltham, Massachusetts: Academic Press; 1990. p. 50–68.
25. May WA, Grigoryan RS, Keshelava N, Cabral DJ, Christensen LL, Jenabi J, et al. Characterization and drug resistance patterns of Ewing's sarcoma family tumor cell lines. PLoS ONE 2013;8:e80060.
26. Ozkaynak MF, Nolta J, Parkman R. In vitro purging of human rhabdomyosarcoma cells using 4-hydroperoxycyclophosphamide. Cancer Res 1990;50:1455–8.
27. Kouraklis G, Triche TJ, Wesley R, Tsokos M. Myc oncogene expression and nude mouse tumorigenicity and metastasis formation are higher in alveolar than embryonal rhabdomyosarcoma cell lines. Pediatr Res 1999;45:552–8.
28. Taylor AC, Shu L, Danks MK, Poquette CA, Shetty S, Thayer MJ, et al. P53 mutation and MDM2 amplification frequency in pediatric rhabdomyosarcoma tumors and cell lines. Med Pediatr Oncol 2000;35:96–103.
29. Keshelava N, Zuo JJ, Chen P, Waidyaratne SN, Luna MC, Gomer CJ, et al. Loss of p53 function confers high-level multidrug resistance in neuroblastoma cell lines. Cancer Res 2001;61:6185–93.
30. Tomayko MM, Reynolds CP. Determination of subcutaneous tumor size in athymic (nude) mice. Cancer Chemother Pharmacol 1989;24:148–54.

31. Frgala T, Kalous O, Proffitt RT, Reynolds CP. A fluorescence microplate cytotoxicity assay with a 4-log dynamic range that identifies synergistic drug combinations. Mol Cancer Ther 2007;6:886–97.
32. Kang MH, Smith MA, Morton CL, Keshelava N, Houghton PJ, Reynolds CP. National cancer institute pediatric preclinical testing program: model description for in vitro cytotoxicity testing. Pediatr Blood Cancer 2010;56:239–49.
33. Kang MH, Wan Z, Kang Y, Sposto R, Reynolds CP. Mechanism of synergy of N-(4-hydroxyphenyl)retinamide and ABT-737 in acute lymphoblastic leukemia cell lines: Mcl-1 inactivation. J Natl Cancer Inst 2008;100: 580–95.
34. Grigoryan R, Keshelava N, Maurer BJ, Sun BC, Ludeman SM, Colvin OM, et al. Cyclophosphamide, but not melphalan or carboplatin, synergistically enhanced topotecan activity against Ewing's family tumor cell lines in hypoxia. Proc Amer Assoc Cancer Res 2005;46:4712.
35. Satoh T, Hosokawa M. The mammalian caboxylesterases: from molecules to functions. Annu Rev Pharmacol Toxicol 1998;38:257–88.
36. Akimoto K, Kawai A, Ohya K. Kinetic-studies of the hydrolysis and lactonization of camptothecin and its derivatives, Cpt-11 and Sn-38, in aqueous-solution. Chem Pharm Bull (Tokyo) 1994;42:2135–8.
37. Loos WJ, Verweij J, Gelderblom HJ, de Jonge MJ, Brouwer E, Dallaire BK, et al. Role of erythrocytes and serum proteins in the kinetic profile of total 9-amino-20(S)-camptothecin in humans. Anticancer Drugs 1999; 10:705–10.
38. Allen TM, Cullis PR. Drug delivery systems: entering the mainstream. Science 2004;303:1818–22.
39. Mayer LD, Janoff AS. Optimizing combination chemotherapy by controlling drug ratios. Mol Intervent 2007;7:216–23.
40. Torchilin VP. Targeted pharmaceutical nanocarriers for cancer therapy and imaging. Aaps J 2007;9:E128–E147.
41. al-Sarireh B, Eremin O. Tumour-associated macrophages (TAMS): disordered function, immune suppression and progressive tumour growth. J R Coll Surg Edinb 2000;45:1–16.
42. Guichard S, Terret C, Hennebelle I, Lochon I, Chevreau P, Frétigny E, et al. CPT-11 converting carboxylesterase and topoisomerase I activities in tumour and normal colon and liver tissues. Br J Cancer 1999;80:364–70.
43. Xu G, Zhang W, Ma MK, McLeod HL. Human carboxylesterase 2 Is commonly expressed in tumor tissue and is correlated with activation of irinotecan. Clin Cancer Res 2002;8:2605–11.
44. Czuprynski CJ, Brown JF. Phagocytes from flora-defined and germfree athymic nude mice do not demonstrate enhanced antibacterial activity. Infect Immun 1985;50:425–30.
45. Kauer M, Ban J, Kofler R, Walker B, Davis S, Meltzer P, et al. A molecular function map of Ewing's sarcoma. PLoS ONE 2009;4:e5415.
46. Chen LT, Shiah HS, Lin PC, Lee JC, Su WC, Wang YW, et al. Phase I study of biweekly liposome irinotecan (PEP02, MM-398) in metastatic colorectal cancer failed on first-line oxaliplatin-based chemotherapy. J Clin Oncol 2012;30:613.

Clinical Cancer Research

Activity of MM-398, Nanoliposomal Irinotecan (nal-IRI), in Ewing's Family Tumor Xenografts Is Associated with High Exposure of Tumor to Drug and High *SLFN11* Expression

Min H. Kang, Jing Wang, Monish R. Makena, et al.

Clin Cancer Res 2015;21:1139-1150.